Structure of the $Na_xCl_{x+1}^-$ ($x=1-4$) clusters via *ab initio* genetic algorithm and photoelectron spectroscopy

Anastassia N. Alexandrova and Alexander I. Boldyrev[a)]
Department of Chemistry and Biochemistry, Utah State University, Logan, Utah 84322-0300

You-Jun Fu, Xin Yang, Xue-Bin Wang, and Lai-Sheng Wang[b)]
Department of Physics, Washington State University, Richland, Washington 99352
and W. R. Wiley Environmental Molecular Sciences Laboratory,
Pacific Northwest National Laboratory, Richland, Washington 99352

(Received 15 June 2004; accepted 25 June 2004)

The application of the *ab initio* genetic algorithm with an embedded gradient has been carried out for the elucidation of global minimum structures of a series of anionic sodium chloride clusters, $Na_xCl_{x+1}^-$ ($x=1-4$), produced in the gas phase using electrospray ionization and studied by photoelectron spectroscopy. These are all superhalogen species with extremely high electron binding energies. The vertical electron detachment energies for $Na_xCl_{x+1}^-$ were measured to be 5.6, 6.46, 6.3, and 7.0 eV, for $x=1-4$, respectively. Our *ab initio* gradient embedded genetic algorithm program detected the linear global minima for $NaCl_2^-$ and $Na_2Cl_3^-$ and three-dimensional structures for the larger species. $Na_3Cl_4^-$ was found to have C_{3v} symmetry, which can be viewed as a Na_4Cl_4 cube missing a corner Na^+ cation, whereas $Na_4Cl_5^-$ was found to have C_{4v} symmetry, close to a 3×3 planar structure. Excellent agreement between the theoretically calculated and the experimental spectra was observed, confirming the obtained structures and demonstrating the power of the developed genetic algorithm technique. © *2004 American Institute of Physics.*
[DOI: 10.1063/1.1783276]

I. INTRODUCTION

Due to their relatively simple potentials dominated by the coulomb interaction, alkali halide clusters have been extensively investigated.[1–7] Systematic studies of the $M_xX_{x+1}^-$ anions with an excess halide anion allow us to trace how the delocalization of the extra charge from the additional X^- affects the electronic and geometric structure of these species. The smallest MX_2^- anions (where $M=$Na, Li, K, Rb, Cs; $X=$F, Cl, Br, I) have been predicted to possess very high electron detachment energies,[8–12] substantially higher than anions of the halogen atoms,[13] and therefore they have been called as ''superhalogens.''[8] Recently, Wang and co-workers have experimentally proved for the first time that the MX_2^- anions indeed have very high vertical electron detachment energies (VDEs) with the highest experimentally measured value to be 5.92 ± 0.04 eV for $LiCl_2^-$.[14] There are a couple of reasons why the MX_2^- anions have very high electron binding energies. One is due to the coordination of X^- to the electropositive M^+ in the ionic M^+X^- molecule and the other is due to the delocalization of the extra charge. One would expect that as the number of atoms in the anionic $M_xX_{x+1}^-$ clusters increases, the electron binding energies of the clusters would keep increasing. An interesting question arises: how high an electron binding energy can one attain in the anionic $M_nX_{n+1}^-$ clusters and what kind of structures will these clusters have?

Using a flowing afterglow discharge ion source, Miller and Lineberger[15] produced clusters of $Na_xF_{x+1}^-$, as well as $Na_{x+1}F_x^-$ and $Na_xF_x^-$ with $x\leqslant17$. But they were not able to photodetach $Na_xF_{x+1}^-$ anions with the available 2.540 eV photons. A series of experimental studies on sodium chloride clusters detected that such systems typically have only one energetically favorable morphology, and the magic numbers appearing in mass spectra correspond to cuboidal fragments of the crystal lattice.[16–18] Bloomfield and co-workers have studied extensively the alkali halide clusters using mass spectrometric and photodetachment techniques.[18–23] Using ion mobility experiment, Jarrold and co-workers were able to assign cuboidal shapes to most of the $Na_xCl_{x+1}^-$ clusters ($x>30$).[24] The structure of anionic sodium chloride clusters, $Na_xCl_{x+1}^-$ clusters (x up to 35), has been previously calculated by Doye and Wales, who used the ''basin hopping'' Monte Carlo minimization technique with two different empirical potentials.[25] Phillips, Conover, and Bloomfield also calculated the structures of $Na_xCl_{x+1}^-$ for $x=2-14$ by Monte Carlo simulation.[26] However, photoelectron spectroscopy (PES) has not been used to study the $Na_xCl_{x+1}^-$ clusters with $x>1$ because of their anticipated high electron binding energies.[8,9,12,14]

In this paper we present an investigation of the electronic and geometric structure of the $Na_xCl_{x+1}^-$ clusters ($x=1-4$) via the *ab initio* gradient embedded genetic algorithm (GEGA) for heteroatomic systems and PES at 157 nm (7.866 eV). The GEGA program for the elucidation of global minimum structures of homoatomic systems has been re-

[a)]Electronic mail: boldyrev@cc.usu.edu
[b)]Electronic mail: ls.wang@pnl.gov

cently reported.[27] This program has been applied for the search for global minima of the $Li_n^{0,+1,-1}$ $(n=5-7)$ clusters. The algorithm reported here is designed specifically for heteroatomic systems. The structures thus obtained are exposed to more accurate theoretical treatment and their computed spectra are compared with the experimental PES spectra, which revealed that indeed the electron binding energies of the $Na_xCl_{x+1}^-$ increase with the cluster size and reaches 6.9 eV for $Na_4Cl_5^-$.

II. EXPERIMENTAL METHOD

The experiment was carried out with a PES apparatus equipped with a magnetic-bottle time-of-flight photoelectron analyzer and an electrospray ionization (ESI) source. Details of the experimental method have been given elsewhere.[28] ESI has been shown to be a suitable source to produce sodium chloride cluster anions previously.[29–32] Briefly, the anions of interest, $Na_xCl_{x+1}^-$, were produced from a solution of sodium chloride (10^{-4} mol/l) in a mixed solvent of $CH_3CN:H_2O=9:1$ by ESI at a high voltage bias of -2.2 kV. Anions produced from the ESI source were guided by a radio-frequency quadruple ion guide into a three-dimensional (3D) quadruple ion-trap, where ions were accumulated for 0.1 s before being pulsed into the extraction zone of a time-of-flight mass spectrometer. The species to be studied were mass selected and decelerated before being intercepted by a probe laser beam in the photodetachment zone of the magnetic-bottle photoelectron analyzer. In the current study, the detachment photon energy 157 nm (7.866 eV) from a F_2 excimer laser was employed. Photoelectrons were collected at nearly 100% efficiency by the magnetic bottle and analyzed in a 4 m long electron flight tube. Photoelectron time-of-flight spectra were collected and then converted to kinetic energy spectra, calibrated by the known spectra of I^- and O^-. The electron binding energy spectra presented here were obtained by subtracting the kinetic energy spectra from the detachment photon energies. The energy resolution $(\Delta E/E)$ was about 2%, i.e., 10 meV for ~0.5 eV electrons, as measured from the spectrum of I^- at 355 nm.

III. THEORETICAL METHODS

We first performed the search for the global minima on the potential energy surface (PES) for systems from $NaCl_2^-$ to $Na_4Cl_5^-$ using the GEGA program (described in detail in the Sec. IV), written by Alexandrova. At this stage we used a mixture of Hartree-Fock exchange with density functional exchange-correlation potentials (B3LYP) (Refs. 33–35) level of theory with 3-21G basis set. The found low-energy structures were further characterized at higher levels of theory. The B3LYP method with the 6-311+G* basis set and TZV- basis set[36,37] extended by addition of *d* functions on all atoms was employed for the geometry optimization and vibrational frequencies calculations [*d*-exponents optimized for NaCl at the CCSD(T)/TZV+*d* level of theory were found to be $\alpha(\mathrm{Na})_d=0.14$, $\alpha(\mathrm{Cl})_d=0.54$]. Geometries and frequencies of smaller systems were also refined using the coupled cluster method [CCSD(T)] (Refs. 38–40) with the same two basis sets 6-311+G* and TZV(+*d*). Theoretical photoelectron spectra were calculated using the restricted outer valence Green-Function method (ROVGF) (Refs. 41–44) with the 6-311+G(2*df*) and TZV(+2*df*) basis sets [$\alpha(\mathrm{Na})_d=0.14$, $\alpha(\mathrm{Na})_d=0.043$, $\alpha(\mathrm{Na})_f=0.185$, $\alpha(\mathrm{Cl})_d=0.54$, $\alpha(\mathrm{Cl})_d=0.18$, $\alpha(\mathrm{Cl})_f=0.65$]. All B3LYP and CCSD(T) calculations were performed using the GAUSSIAN 03 program.[45] The ROVGF calculations were done using the GAUSSIAN 98 package.[46]

IV. GENETIC ALGORITHM

The GEGA is an optimization strategy based on the Darwinian evolution process.[47] Genetic algorithms (GAs), simple methods which do not include the calculations of derivatives, were successfully used in many areas of science and technology when global optima for complex, many-parameter functions need to be found.[48,49] The GA based strategy for the search of the global minima of clusters has been previously shown to be an effective technique, and many different approaches of such application of the GA have been reported.[50–72]

The GA based search for the global minimum is performed in the $3N$-6 configurational space with energy value as a criterion of the fit. All the structures generated during the GEGA execution are being optimized to the nearest stationary point using the conventional gradient techniques (GAUSSIAN 03 package is employed for all calculations). Then the Algorithm runs a frequency calculation in order to check if the stationary point is a local minimum or a saddle point. If the stationary point is a saddle point, then the algorithm continues the optimization following the mode of the largest imaginary frequency until the local minimum is found. The hybrid B3LYP method, which is a relatively computationally cheap, with a small 3-21G basis set is used throughout the execution. Many works on the search for global minima of clusters have been reported,[50–72] including ones involving single-point energy calculations and ones based on the gradient-following technique. The Lennard-Jones and other types of empirical potentials were used to evaluate the energies or to optimize geometries. The density-functional method with the local density approximation was used in the modified GA proposed by Tomasulo and Ramakrishna,[62] for $(\mathrm{AlP})_n$ clusters. However, the authors used the structures of the isoelectronic silicon clusters as an initial guess for the $(\mathrm{AlP})_n$ clusters, and the GA itself was based on mutations only and did not include the full conventional mating operations. This work presents a cooperative application of the GA features, of the gradient-following technique implemented to GAUSSIAN03 and of the power of the modern *ab initio* calculations to the search for global minima of heteroatomic clusters.

A. Generation of the population

The first step of the GEGA algorithm is to create an initial population of individuals. For every initial individual we randomly generated Cartesian coordinates within the 3 dimensional sphere from zero to the maximum distance *R*, calculated on the basis of the user-defined average interatomic distance within the cluster. The minimum interatomic distance, also given by the user, is kept to prevent any two

atoms from being too close to each other within the generated species. Since the three-dimensional random coordinate generation leaves a very small chance for planar or linear species to be chosen, several steps of the creation of the population are done to accelerate the convergence of the GA. First a random population of linear individuals is created by random generation of N x coordinates of N individuals with their $y=z=0$. Based on the calculated single-point energies, the N best-fit individuals are chosen, where N is the population size defined by the user. Fifty individuals are the recommended size of the population for the systems containing up to ten atoms, in agreement with the previously reported recommendation.[51] On the second step planar species are added to the population. Their abundance is much larger, since the variational freedom is increased in comparison with single-dimensional (1D) linear isomers (x and y are generated randomly, while $z=0$ for each species). The competition between single-point energies of linear and planar individuals forms the new population of the size N. After that 3D species are thrown into the population by the random generation of $3N$ coordinates of each species. The N best-fit species are selected, again reconstructing the requested size of the population. The range of random variation of the atomic coordinates is adjusted to the dimensionality for more efficient performance: 1D species have larger range of variation of coordinates than 2D ones, and 2D individuals have a larger range than 3D ones, which are expected to have the most compact geometries. Thus the constructed initial selection gives sufficient saturation of the population with planar, linear, and three-dimensional species. The initial selection stage is somewhat reminiscent of the Monte Carlo simulation,[73] since it involves a simple trial random generation of configurations and further choosing of the best-fit individuals. This technique demonstrated itself to be effective for the overall faster convergence of the algorithm.

On the next step a geometry optimization to the nearest local minimum of all preselected species is performed. In earlier works the gradient-following technique was employed for the search for global minima of clusters.[52,53,59] White and co-authors[53] proved the high efficiency of the gradient-following technique in comparison to simple GA procedures. One of the major problems of any GA technique is the chance of getting stuck in a local minimum and never finding the global minimum. The probability of ending up in one of the local minima is decreased by saturating the population with a large number of good solutions, which are the local minima.

B. Breeding

For the consequent breeding process each prepared species is assigned a certain probability to breed according to its position in the list of species, which is composed on the basis of the fit criterion. The so-called ''gambling-circle'' technique is introduced for the mate selection. The robust mating technique proposed by Deaven and Ho[59] is then employed. For the pair of selected parents the cutting plane is then randomly chosen between xy, yz, and zx. And the halves of the parents are recombined in a child. Coordinates of parents are taken from the GAUSSIAN output file in the form of standard orientation, in which the centers of mass of species are at the origin and their orientation in space is arbitrary due to the low symmetry. Arbitrary orientation introduces the randomness in the cutting process, thus allowing us to restrict the group of mating operators to the simple and the head-to-tail mating operators and the collection of cutting planes to xy, yz, and xz, although a quite large variety of mating operators was proposed.[69,74,75] In our algorithm the chance of selecting the simple or the head-to-tail mating way is 50%. Kabrede and Hentschke proposed the ''self-training'' selection of mating operators,[75] in which the efficiency of a mating operator is checked on each step and the probability of this operator to be chosen in the future is thus determined. We keep the choosing probability constant because the efficiency of an operator in one case of mating may not be relevant to another one, and lowering the probability of selecting an operator makes the outcomes from further steps of breeding unpredictable. After the breeding the resulting number of atoms of all types in the child is checked. If after the recombination it is found that the cluster has a wrong number of atoms, the second parent is shifted with respect to the cutting plane and the second half of the genes is taken again.

The new species thus carries the features of both parents. If it happens that both times the same parent is being selected in the act of breeding or if the parents are identical, the resulting child is mutated, as it is reasonable to expect in real life. Created offspring are further exposed to the geometry optimization to the nearest local minima on the potential energy surface.

Each couple of parents has one offspring in each step of the execution. The gamblinglike selection of parents and breeding continues until the number of species N in the population is duplicated: there are N initial parents plus N newborn children. The new selection of the N best-fit species is performed. On each step of the algorithm the current lowest-energy structure is detected. If the number of iterations of breeding, within which the same structure remains the current global minimum, reaches 20, the Algorithm is considered converged to the actual global minimum or to a very stable, good local minimum. If convergence was not yet met the mutation process occurs.

C. Mutations

There are two special features of the mutation process implemented: the drastic geometry change of the mutant and the high percentile of mutations. Mutations are performed on the highest energy (the worst fitting) species in the population. The mutations are the shifts of a random number of atoms (no smaller than 3) in the cluster in random directions (x, y, or z). The user sets the maximum mutation shift value, since the necessary shifting is different for different systems. The ''respect'' interatomic distance is ''kept in mind'' during the mutation process, so that if any two atoms happen to occur too close to each other, mutation shift is decreased for one of them and the new check of ''respect'' is organized. The mutants are optimized to the nearest local minima and added to the population along with their precursors. Because the optimization of mutants is implemented, slight mutations cannot affect the configuration, as the geometry optimization

of a slightly mutated species will simply get it down to the same local minimum and no valuable change will happen in the population. Thus, in order to push a species out of the current well on the potential energy surface, we made mutations to lead to a drastic change in the geometry of mutants, introducing the features of the stochastic algorithm suggested by Saunders.[76]

Usually the mutation rate for the genetic algorithm is recommended to be between 10% and 15% of the population to model the natural mutations that occur in real life. However, we set the mutation rate to 1/3 of the population (i.e., 33.33%), which was shown to be efficient for the thus organized search for global minima. During the mutation process there is always a chance for the mutant to end up in the local minimum, from which it originates, and thus, the effective mutation rate is actually lower than the preset 33.33%.

Instead of substituting the mutating species with the mutants according to the conventional GA method, we leave both groups of species in the population. This is done because both the initial structures and the mutants in most of the cases are different local minima on the potential energy surface and can be different good solutions. At the end of the mutation process, we allow all the species to compete for survival, and the N size of the population is reconstructed in the sorting process. After mutating of the population, a new iteration of breeding, check convergence, and mutations occurs.

D. Final output

When convergence is met there can be two possibilities for the resulting population. It may contain the global minimum structure with or without other low-lying isomers that survived throughout the breeding and mutations. Alternatively, the run may result in a local minimum species. In this case the population will contain this very stable local minimum with or without some other isomers and will not contain the global minimum. In the first case one often may wish to have information about all low-energy isomers without omitting any of them, as they can be valuable isomers and can even have lower energies at the higher level of theory. This issue has been resolved through the saving of low-energy species (differing from the current minimum energy species by no more than 10 kcal/mol) in a ''bank'' of species available for the user as well as for the final sorting engine on each of the iterations of the algorithm.

To prevent the user from being misled by the wrong answer in the second outcome mentioned above, we recommend running the GA independently several times for the same cluster. This way, if one of the calculations has become stuck in a local minimum, another run may lead to the right answer, and if all runs give the same result there is then reason for some certainty in the obtained global minimum geometry.

At the end of the execution the finalists and the species from the bank are classified according to the difference of their energies from the global minimum. The geometries of species having energies different from the global minimum by no more than 1 kcal/mol are further checked for geometrical identity with the global minimum. It is specifically reported if a different very low-energy isomer is found.

E. Specifics of the algorithm

The following information is requested from the user at the beginning of the execution: types and numbers of atoms in the cluster, charge and multiplicity, average interatomic distance, minimum interatomic distance allowed (the respect distance), maximum mutation shift value, and number of individuals in the population. Usually the real global minimum can be found within three to five cycles of breeding and mutations. Nineteen additional cycles are run to check if the convergence criterion is met. Thus 23–25 runs of the algorithm are needed to get the stable answer of a particular run. Usually genetic algorithms converge a lot slower (it was shown that hundreds or even thousands of iterations are required to meet the convergence criterion). We would like to point out this great advantage of using GA features together with the following gradient *ab initio* calculations. The other way the GA can be terminated is if 500 iterations are done but the global minimum is still undefined. This can happen if the initial parameters (such as the minimum and the average interatomic distances, the mutation shift, or the population size) were not specified properly.

As always in the GA based techniques, some uncertainty is present in the performance. The user has to manipulate the input parameters to find the optimum for the particular problem. Also some critical review of the obtained results is always needed. The user should vary the input parameters and run the same job two to three times independently to be sure of the resulting answer.

There is also a restriction on the multiplicity of the cluster. For systems tended to have various multiplicity values several runs of the GA with different multiplicity requests are needed. For simpler systems it may be more reasonable to run individual calculations for the lowest energy isomers with different multiplicities. In our case we have only run GEGA for singlet states of $Na_xCl_{x+1}^-$.

V. EXPERIMENTAL RESULTS

Figure 1 shows the PES spectra of $Na_xCl_{x+1}^-$ ($x=1-4$) taken at 157 nm. The spectrum of $NaCl_2^-$ showed three bands (X,A,B) [Fig. 1(a)]. This species has been reported previously at 193 nm (6.424 eV) and the current spectrum agrees with the previous 193 nm data[5] except that a very high binding energy band (B) at a VDE of 7.74 eV was observed in the current spectrum. As shown previously, the broadband X in fact contained three detachment channels or five final electronic states if spin-orbit splitting is taken into account. Due to the overlapping nature of all these states, their VDEs could not be accurately determined from the current data. A VDE of 5.6 eV was estimated for of $NaCl_2^-$, consistent with the previous measurement at 193 nm. Band A at 6.39 eV and band B at 7.74 eV are relatively sharp and should correspond to single electronic transitions. Band A was observed in the previous 193 nm data as a very weak feature, but its relative intensity seemed to be enhanced in the current 157 nm spectrum.

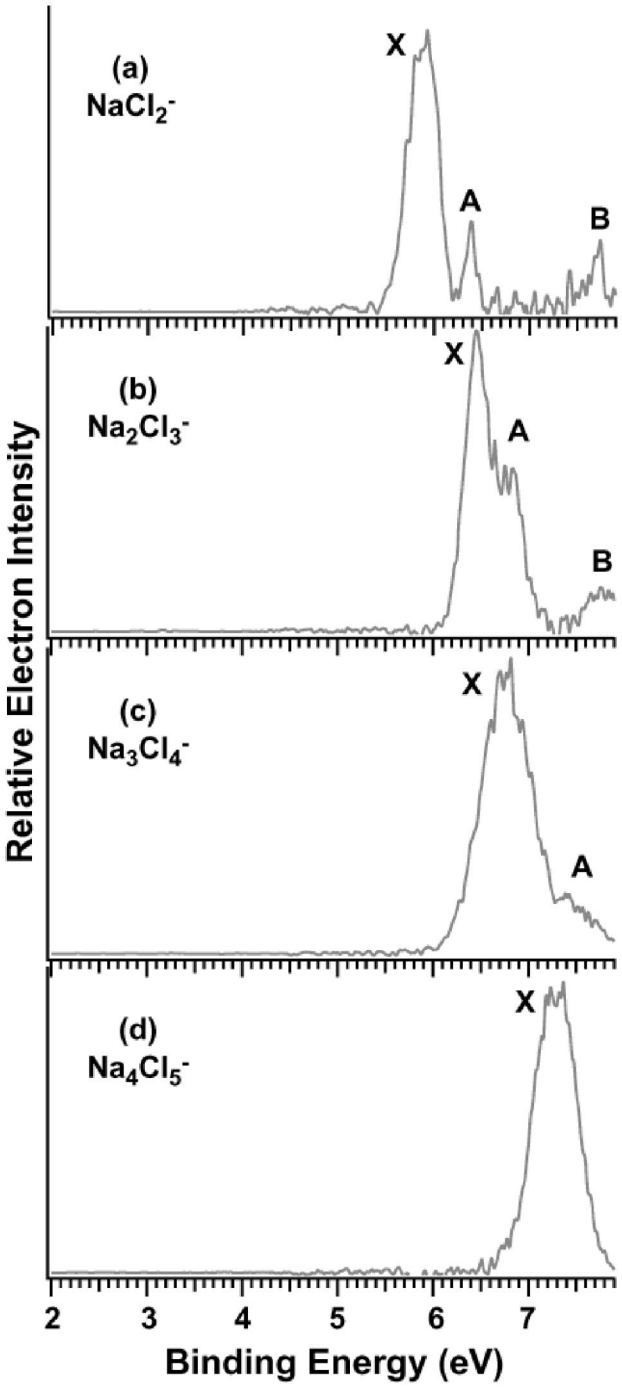

FIG. 1. Photoelectron spectra of $Na_xCl_{x+1}^-$ ($x=1-4$) at 157 nm (7.866 eV).

Three bands were observed in the spectrum of $Na_2Cl_3^-$ [*X*, *A*, *B*, Fig. 1(b)]. The band *B* at the high binding energy side was relatively weak. The binding energies of $Na_2Cl_3^-$ are significantly increased. The first VDE of 6.46 eV was measured from the spectrum. The spectrum of $Na_3Cl_4^-$ was considerably broader [Fig. 1(c)], while its binding energies were only slightly increased relative to those of $Na_2Cl_3^-$. The weak *A* band of $Na_3Cl_4^-$ was also relatively broad. Only one broadband was observed for $Na_4Cl_5^-$ [Fig. 1(d)]. The binding energies of $Na_4Cl_5^-$ were significantly increased relative to $Na_3Cl_4^-$. The first VDE of 7.0 eV was estimated for

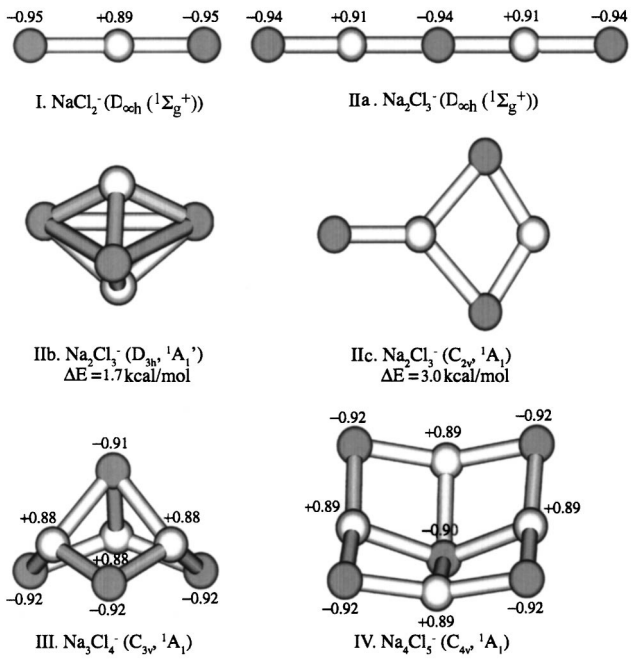

FIG. 2. Lowest-energy structures of the $Na_xCl_{x+1}^-$ clusters ($x=1-4$) found by the GEGA program. The ΔE values are given at the CCSD(T)/6-311+G($2df$) level of theory, and NPA effective charges are given at the B3LYP/6-311+G* level of theory.

$Na_4Cl_5^-$. The binding energies of the $Na_xCl_{x+1}^-$ clusters will be compared with the theoretical calculations next.

We note that the spectral features of $NaCl_2^-$ and $Na_2Cl_3^-$ are relatively sharp, whereas those of $Na_3Cl_4^-$ and $Na_4Cl_5^-$ are relatively broad, suggesting that there might be a structural transition from $Na_2Cl_3^-$ to $Na_3Cl_4^-$. We note that $NaCl_2^-$ has a $Cl^-Na^+Cl^-$ linear structure from our previous work.[14] The relatively sharp spectral features of $Na_2Cl_3^-$ might suggest that it also has a linear structure, $Cl^-Na^+Cl^-Na^+Cl^-$, whereas a linear to planar or three-dimensional structure transition takes place at $Na_3Cl_4^-$. As will be discussed below, these expectations are born out from our theoretical calculations.

VI. THEORETICAL RESULTS

The GEGA program revealed the global minimum structures of the $NaCl_2^-$, $Na_2Cl_3^-$, $Na_3Cl_4^-$, and $Na_4Cl_5^-$ clusters. The smaller $NaCl_2^-$ and $Na_2Cl_3^-$ clusters were found to have linear shapes, while bigger systems prefer more compact three-dimensional structures in their most stable form, consistent with the expectations from the photoelectron spectra presented above. The global minima and low-lying isomers (differing from the global minima by no more than 10 kcal/mol) are shown in Fig. 2 for $Na_xCl_{x+1}^-$ ($x=1-4$).

In the case of the linear clusters, 20 cycles of the GEGA execution reached the global minimum structures. In fact the global minima were found on the very first cycle of the algorithm. This was achieved by the three-step generation of the initial population. As it has been mentioned, linear species are purposely included into the population at the first step of the algorithm. Apparently, the proper sequences of

TABLE I. Molecular properties of $NaCl_2^-$.

Method	B3LYP/3-21G	B3LYP/6-311+G*	B3LYP/TZV(+*d*)	CCSD(T)/6-311+G*	CCSD(T)/TZV(+*d*)
Etotal (a.u.)	−1077.523 603	−1082.985 962	−784.909 436	−1081.971 322	−1081.390 997
Nimag	0	1	0	0	0
ZPE (kcal/mol)	1.050	1.014	0.625	1.060	0.990
R(Na-Cl) (Å)	2.48	2.51	2.55	2.49	2.51
$\omega_1(\pi_u)$ (cm^{-1})[a]	91 (43)	90 (48)	39 i(30)	90	79
$\omega_2(\sigma_g)$ (cm^{-1})[a]	187 (0)	181 (0)	180 (0)	191	188
$\omega_3(\sigma_u)$ (cm^{-1})[a]	365 (41)	342 (92)	259 (223)	366	347

[a]Infrared intensities are shown in parentheses.

TABLE II. (a) Molecular properties of the $D_{\infty h}(^1\Sigma_g^+)$ $Na_2Cl_3^-$ global minimum structure (IIa, Fig. 2). (b) Molecular properties of the $D_{3h}(^1A_1')$ $Na_2Cl_3^-$ isomer (IIb, Fig. 2). (c) Molecular properties of the $C_{2v}(^1A_1)$ $Na_2Cl_3^-$ isomer (IIc, Fig. 2).

Method	B3LYP/3-21G	B3LYP/6-311+G*	B3LYP/TZV(+*d*)	CCSD(T)/6-311+G*	CCSD(T)/TZV(+*d*)
(a) Etotal (a.u.)	−1696.958 327	−1705.647 036	−1705.626 585	−1703.051 188	−1703.046 729
ΔE (kcal/mol)	0	0	0	0	0
NImag	0	0	0	1	0
ZPE (kcal/mol)	2.068	2.113	1.910	1.988	1.860
$R(Cl_1\text{-}Na_2)$ (Å)[b]	2.50	2.55	2.54	2.54	2.56
$R(Na_2\text{-}Cl_3)$ (Å)[c]	2.46	2.47	2.47	2.46	2.49
$\omega_1(\pi_u)$ (cm^{-1})[a]	97 (82)	127 (76)	79 (84)	91	74
$\omega_2(\pi_u)$ (cm^{-1})[a]	14 (3)	25 (11)	13 (4)	10 i	3
$\omega_3(\pi_g)$ (cm^{-1})[a]	75(0)	79 (0)	65(0)	73	62
$\omega_4(\sigma_u)$ (cm^{-1})[a]	380 (101)	355 (186)	356 (141)	371	356
$\omega_5(\sigma_u)$ (cm^{-1})[a]	223 (1)	214 (1)	217(1)	221	218
$\omega_6(\sigma_g)$ (cm^{-1})[a]	354 (0)	337 (0)	338 (0)	397	339
$\omega_7(\sigma_g)$ (cm^{-1})[a]	118 (0)	111 (0)	113 (0)	115	114
(b) Etotal (a.u.)	−1696.955 937	−1605.637 640	−1705.622 460	−1703.047 994	−1703.041 395
ΔE (kcal/mol)	1.5	5.9	2.6	2.0	3.3
Nimag	0	0	0	0	0
ZPE (kcal/mol)	2.324	2.186	2.271	2.225	2.290
R(Na-Cl) (Å)	2.65	2.66	2.66	2.64	2.66
R(Cl-Cl) (Å)	3.95	3.98	3.96	3.91	3.96
$\omega_1(a_1')$ (cm^{-1})[a]	243 (0)	251 (0)	258 (0)	268	256
$\omega_2(a_1')$ (cm^{-1})[a]	154 (0)	163 (0)	169 (0)	168	171
$\omega_3(a_2'')$ (cm^{-1})[a]	193 (90)	186 (94)	194 (106)	199	192
$\omega_4(e')$ (cm^{-1})[a]	242(67)	222 (106)	231 (105)	243	256
$\omega_5(e')$ (cm^{-1})[a]	110 (16)	96 (12)	103 (14)	100	105
$\omega_6(e'')$ (cm^{-1})[a]	166 (0)	146 (0)	151 (0)	166	154
(c) Etotal (a.u.)	−1696.954 179	−1705.638 142	−1705.621 087	−1703.046 188	−1703.040 521
ΔE (kcal/mol)	8.88	5.58	3.45	3.14	3.90
Nimag	0	0	0	0	0
ZPE (kcal/mol)	2.139	2.037	2.101	2.160	2.112
$R(Cl_1\text{-}Na_2)$ (Å)[d]	2.51	2.53	2.51	2.51	2.52
$R(Na_2\text{-}Cl_{3,4})$ (Å)[e]	2.79	2.83	2.81	2.76	2.81
$R(Na_2\text{-}Na_5)$ (Å)[f]	3.38	3.34	3.31	3.33	3.34
$\langle(Cl_3\text{-}Na_2\text{-}Na_4)$	46.3°	46.5°	46.6°	46.7°	46.5°
$\omega_1(a_1)$ (cm^{-1})[a]	306 (28)	283 (44)	293 (38)	305	298
$\omega_2(a_1)$ (cm^{-1})[a]	270 (52)	265 (69)	271 (67)	279	273
$\omega_3(a_1)$ (cm^{-1})[a]	135 (15)	121 (21)	130 (22)	133	130
$\omega_4(a_1)$ (cm^{-1})[a]	108 (4)	100 (3)	104 (3)	103	104
$\omega_5(b_1)$ (cm^{-1})[a]	114 (66)	110 (60)	111 (70)	115	115
$\omega_6(b_1)$ (cm^{-1})[a]	42 (7)	42 (6)	40 (6)	42	40
$\omega_7(b_2)$ (cm^{-1})[a]	316 (42)	317 (71)	325 (65)	330	327
$\omega_8(b_2)$ (cm^{-1})[a]	145 (26)	123 (40)	132 (42)	144	132
$\omega_9(b_2)$ (cm^{-1})[a]	61 (3)	61 (2)	64 (2)	59	62

[a]Infrared intensities are shown in parentheses.
[b]Cl_1 is a central Cl atom.
[c]Cl_3 is a peripheral Cl atom.
[d]Cl_1 is an atom coordinated to the 4-membered Na_2Cl_2 cycle.
[e]$Cl_{3,4}$ are atoms in the y-membered Na_2Cl_2 cycle.
[f]Na_2 is an atom in the u-membered Na_2Cl_2 cycle with the coordination number 2.

TABLE III. Molecular properties of $Na_3Cl_4^-$ $C_{3v}(^1A_1)$ global minimum isomer.

Method	B3LYP/3-21G	B3LYP/6-311+G*	B3LYP/TZV(+d)	CCSD(T)/6-311+G*	CCSD(T)/TZV(+d)
Etotal (a.u.)	−2316.427 350	−2328.323 246	−2328.307 640	−2324.732 943	−2324.718 443
Nimag	0	0	0	a	a
ZPE (kcal/mol)	3.615	3.425	3.534	a	a
$R(Cl_1\text{-}Na_{2,3,4})$ (Å)	2.72	2.70	2.69	2.67	2.70
$R(Cl_1\text{-}Cl_{5,6,7})$ (Å)	3.94	3.95	3.94	3.90	3.93
$\langle(Na_2\text{-}Cl_1\text{-}Na_3)$ (deg)	76.2	75.3	75.3	75.8	75.9
$\langle(Cl_6\text{-}Cl_1\text{-}Cl_5)$ (deg)	74.6	74.5	74.5	75.4	75.2
$\omega_1(a_1)$ $(cm^{-1})^b$	225 (28)	218 (71)	223 (75)	a	a
$\omega_2(a_1)$ $(cm^{-1})^b$	207 (57)	193 (32)	202 (35)	a	a
$\omega_3(a_1)$ $(cm^{-1})^b$	163 (13)	160 (11)	166 (14)	a	a
$\omega_4(a_1)$ $(cm^{-1})^b$	84 (22)	80 (15)	84(18)	a	a
$\omega_5(a_2)$ $(cm^{-1})^b$	243 (0)	224 (0)	231 (0)	a	a
$\omega_6(e)$ $(cm^{-1})^b$	282 (60)	264 (100)	272 (94)	a	a
$\omega_7(e)$ $(cm^{-1})^b$	185 (62)	178 (57)	185 (62)	a	a
$\omega_8(e)$ $(cm^{-1})^b$	164 (4)	154 (1)	160 (3)	a	a
$\omega_9(e)$ $(cm^{-1})^b$	110 (3)	103 (3)	106 (3)	a	a
$\omega_{10}(e)$ $(cm^{-1})^b$	61 (6)	61 (4)	62 (5)	a	a

[a]Frequencies were not calculated at this level of theory.
[b]Infrared intensities are shown in parentheses.

atoms of the linear global minima were chosen among the randomly created linear individuals. Further, during the optimization to the nearest local minima, the needed species were optimized to the global minima structures, having the lowest energy in the population. On the subsequent cycles of the GEGA, these species remained the most stable in the population, and after the 20 cycles the algorithm was considered converged. This nice convergence rate showed the importance of the designed three-step generation of the initial population.

A. $NaCl_2^-$

The GEGA method revealed only one $D_{\infty h}(^1\Sigma_g^+)$ structure (Fig. 2, I), which is the global minimum for the smallest considered cluster $NaCl_2^-$, in agreement with all previous calculations.[1–12,14] Molecular properties of the $NaCl_2^-$ anion at several levels of theory are given in Table I. The B3LYP/3-21G geometry and frequencies were found to be in excellent agreement with more sophisticated calculations CCSD(T)/6-311+G* and CCSD(T)/TZV(+*d*). Surprisingly, we found that the linear structure is not a minimum at the B3LYP/TZV(+*d*) level of theory. Certainly, the B3LYP and TZV(+*d*) combination has a problem with describing the $NaCl_2^-$ anion. However the CCSD(T) calculations with the 6-311+G* or TZV(+*d*) basis sets give very similar results with the linear structure being the global minimum.

B. $Na_2Cl_3^-$

From our GEGA calculations we found three low-lying structures for $Na_2Cl_3^-$: a linear $D_{\infty h}(^1\Sigma_g^+)$ structure (Fig. 2, IIa), a triangular bipyramidal $D_{3h}(^1A_1')$ structure (Fig. 2, IIb), and a planar $C_{2v}(^1A_1)$ structure (Fig. 2, IIc). The linear structure is the global minimum. The calculated molecular properties of all the three isomers are presented in Table II.

The linear structure was found to be the global minimum, except for at the CCSD(T)/6-311+G* level of theory. We believe that the doubly degenerate imaginary frequency for the $D_{\infty h}(^1\Sigma_g^+)$ structure of $Na_2Cl_3^-$ is an artifact of this method. It was already shown before that the CCSD(T)/6-311+G* level of theory gives the $C_{2v}(^1A_1)$ global minimum structure for Na_2O,[77] while the CCSD(T) calculations with more extended basis sets clearly show that the linear structure of Na_2O is the global minimum.[78] Taking into account that the $Na_2Cl_3^-$ anion is linear at all other levels of theory, we conclude that the linear structure is the true global minimum for $Na_2Cl_3^-$, consistent with the experimental expectation. We will see below that calculated VDEs of the linear structure are in a very good agreement with experimental data.

C. $Na_3Cl_4^-$

The GEGA method predicts a three-dimensional structure for $Na_3Cl_4^-$ with $C_{3v}(^1A_1)$ symmetry (Fig. 2, III), consistent with the experimental expectation. In this case, the global minimum was found within 21–23 cycles in the three runs of the GEGA that were performed. The C_{3v} global minimum can be viewed as a fragment of the Na_4Cl_4 cubic structure with one missing corner Na^+. A linear $D_{\infty h}(^1\Sigma_g^+)$ isomer for $Na_3Cl_4^-$ was found to be substantially less stable [13.5 kcal/mol at the CCSD(T)/TZV(+*d*) level]. No other low-lying isomers were found within 10 kcal/mol. The calculated molecular properties of the species are given in Table III.

D. $Na_4Cl_5^-$

Interestingly, in all runs, the global minimum of the larger $Na_4Cl_5^-$ system was reached within 20 cycles of the GEGA. The $Na_4Cl_5^-$ cluster was found to have a quasiplanar 3×3 shape (Fig. 2, IV). This slightly out-of-plane distorted species possesses $C_{4v}(^1A_1)$ symmetry (see Table IV for more detailed computed molecular properties of the species). The key to the fast convergence of the GEGA in this case is also in the method of the generation of the initial population of individuals. Lets take a look at the logically ''see-

TABLE IV. Molecular properties of $Na_4Cl_5^-$ $C_{4v}(^1A_1)$ global minimum isomer.

Method	B3LYP/3-21G	B3LYP/6-311+G*	B3LYP/TZV(+*d*)
Etotal (a.u.)	−2935.883300	−2951.001352	−2950.983565
Nimag	0	0	0
ZPE (kcal/mol)	4.685	4.535	4.653
$R(Cl_1\text{-}Na_{2,3,4,5})$ (Å)	2.71	2.73	2.72
$R(Cl_1\text{-}Cl_{5,6,7,8})$ (Å)	3.91	3.95	3.95
$\langle(Na_2\text{-}Cl_1\text{-}Na_3)$ (deg)	135.9	131.5	131.04
$\langle(Cl_6\text{-}Cl_1\text{-}Cl_5)$ (deg)	135.8	132.2	131.94
$\omega_1(a_1)$ $(cm^{-1})^a$	207 (19)	203 (36)	209 (41)
$\omega_2(a_1)$ $(cm^{-1})^a$	166 (3)	160 (0)	165 (0)
$\omega_3(a_1)$ $(cm^{-1})^a$	135 (111)	132 (77)	137 (92)
$\omega_4(a_1)$ $(cm^{-1})^a$	49 (17)	53 (14)	54 (16)
$\omega_5(a_2)$ $(cm^{-1})^a$	273 (0)	259 (0)	265 (0)
$\omega_6(b_1)$ $(cm^{-1})^a$	307 (0)	294 (0)	300 (0)
$\omega_7(b_1)$ $(cm^{-1})^a$	91 (0)	83 (0)	86 (0)
$\omega_8(b_1)$ $(cm^{-1})^a$	20 (0)	27 (0)	28 (0)
$\omega_9(b_2)$ $(cm^{-1})^a$	156 (0)	153 (0)	159 (0)
$\omega_{10}(b_2)$ $(cm^{-1})^a$	132 (0)	126 (0)	130 (0)
$\omega_{11}(b_2)$ $(cm^{-1})^a$	24 (0)	48 (0)	48 (0)
$\omega_{12}(e)$ $(cm^{-1})^a$	295 (101)	283 (165)	288 (146)
$\omega_{13}(e)$ $(cm^{-1})^a$	210 (60)	191 (50)	198 (52)
$\omega_{14}(e)$ $(cm^{-1})^a$	163 (5)	159 (7)	165 (6)
$\omega_{15}(e)$ $(cm^{-1})^a$	114 (22)	105 (20)	108 (22)
$\omega_{16}(e)$ $(cm^{-1})^a$	77 (2)	79 (1)	79 (1)

[a]Infrared intensities are shown in parentheses.

through'' process of creation, optimization, and confirmation of this global minimum. Initially, the planar shape was chosen on the second step of the generation of the population. Further geometry optimization of the species led to the D_{4h} planar species, which was a first-order saddle point on the potential energy surface. The program indicated the presence of the imaginary frequency in the isomer, and introduced the displacements according to the normal mode of the imaginary frequency. Subsequent geometry optimization led to the final C_{4v} structure, which remained the global minimum for the 19 executed iterations. The convergence rate can vary and it depends on the symmetry of the actual global minimum species, the parameters given by the user, or the fortune of the random geometries initially chosen. Nevertheless, the successful execution for $Na_4Cl_5^-$ was achieved only because of the three-step generation of the population and the following gradient optimization to the nearest local minimum. As in all previous cases, the B3LYP/3-21G level of theory used in the GEGA method gives rather good geometrical parameters as compared to the more sophisticated CCSD(T)/6-311+G* and CCSD(T)/TZV(+*d*) methods. Other local minima have been found substantially higher in energy. For example, one of the most intuitively sound isomers composed of a Na_4Cl_4 cube with Cl^- anion coordinated to one of the Na vertexes has been found to be 15.9 kcal/mol above the global minimum at the B3LYP/TZV (+*d*) level.

Overall, starting from the $Na_3Cl_4^-$ cluster, the $Na_xCl_{x+1}^-$ systems prefer three-dimensional structures in their most stable form, in agreement with the experimental spectral evolution. Calculated effective natural population analysis (NPA) atomic charges (B3LYP/6-311+G*) clearly show predominantly ionic character in all the anionic clusters. The obtained global minimum structures are consistent with those previously found by Monte Carlo method.[25,26]

TABLE V. Experimental and theoretical vertical detachment energies (VDE) in eV of the $NaCl_2^-$ ($D_{\infty h}$, $^1\Sigma_g^+$) global minimum isomer.

			VDE (theoretical)[a]	
Feature	VDE (expt.)	Molecular orbital	ROVGF/*tzv*(+2*df*)	ROVGF/6-311+G(2*df*)
X	5.6–6.1	$1\pi_g$	5.75 (0.92)	5.84 (0.91)
		$1\pi_u$	5.76 (0.92)	5.87 (0.91)
		$2\sigma_u$	5.95 (0.92)	6.06 (0.91)
A	6.39[b]	$2\sigma_g$	6.24 (0.92)	6.35 (0.91)
B	7.74[b]			

[a]Pole strengths are shown in parentheses.
[b]Experimental uncertainty: ±0.04 eV.

TABLE VI. Experimental and theoretical vertical detachment energies (VDE) in eV for the global minimum linear structure and two low-lying isomers of $Na_2Cl_3^-$.

Feature	VDE (expt.)	Molecular orbital	VDE (theoretical)[a] ROVGF/TZV(+2df)[c]	VDE (theoretical)[a] ROVGF/6-311+G(2df)[d]
		$Na_2Cl_3^-(D_{\infty h}, {}^1\Sigma_g^+)$		
X	6.46[b]	$2\pi_u$	6.39 (0.92)	6.49 (0.92)
		$2\pi_g$	6.39 (0.92)	6.49 (0.92)
A	6.84[b]	$3\sigma_u$	6.73 (0.92)	6.84 (0.92)
		$3\sigma_g$	6.76 (0.92)	6.86 (0.91)
B	7.76[e]	$1\pi_u$	7.91 (0.92)	7.93 (0.91)
		$Na_2Cl_3^-(D_{3h}, {}^1A_1')$		
		$1a_2'$	5.72 (0.91)	5.71 (0.91)
		$3e'$	5.90 (0.91)	5.91 (0.91)
		$1e''$	6.21 (0.92)	6.25 (0.91)
		$2e'$	6.39 (0.92)	6.44 (0.91)
		$1a_2''$	6.45 (0.92)	6.50 (0.91)
		$Na_2Cl_3^-(C_{2v}, {}^1A_1)$		
		$4b_2$	5.32 (0.92)	5.34 (0.91)
		$2b_1$	5.33 (0.92)	5.36 (0.91)
		$5a_1$	5.65 (0.92)	5.68 (0.91)
		$1a_2$	6.89 (0.91)	6.89 (0.91)
		$3b_2$	6.89 (0.92)	6.89 (0.91)

[a]Pole strengths are shown in parentheses.
[b]Experimental uncertainty: ±0.04 eV.
[c]At the CCSD(T)/*tzv*(+*d*) geometry.
[d]At the CCSD(T)/6-311+G* geometry.
[e]Experimental uncertainty: ±0.06 eV.

VII. COMPARISON OF EXPERIMENTAL PHOTOELECTRON SPECTRA AND THEORETICAL VDES

Theoretical VDEs were calculated at the ROVGF/6-311+(2*df*) and ROVGF/*tzv*(+2*df*) levels of theory for all the global minima and low-lying isomers shown in Fig. 2. It was previously shown[14,79–81] that the ROVGF/6-311+G(2*df*) method works rather well for superhalogen anions. The experimental VDEs and the theoretically calculated VDEs are compared in Tables V–VIII for $Na_xCl_{x+1}^-$ ($x=1-4$), respectively.

Detailed comparison between experiment and theory of $NaCl_2^-$ was presented in our previous work[14] and it is included here for completeness. For $Na_2Cl_3^-$, we computed the VDEs for all three isomers shown in Fig. 2, as shown in Table VI. Most impressively, only the calculated VDEs of the global minimum linear structure agree with the experimental data. Clearly, the *X* band corresponds to two detachment channels, $2\pi_u$ and $2\pi_g$, which yielded identical VDEs. The *A* band also corresponds to two detachment channels, $3\sigma_u$ and $3\sigma_g$. The fifth detachment channel, at a calculated VDE of 7.9 eV from the linear structure, is from the $1\pi_u$ orbital, and is in excellent agreement with the experimental spectrum.

The calculated spectral pattern of $Na_3Cl_4^-$ is very complicated. We note that there are six detachment channels between 6.68 and 7.14 eV (Table VII), which would give rise to an unresolved broad spectral band. This is in exact agree-

TABLE VII. Experimental and theoretical vertical detachment energies (VDE) in eV for the $Na_3Cl_4^-$ ($C_{3v}, {}^1A_1$) global minimum structure.

Feature	VDE (expt.)	Molecular orbital	VDE (theoretical)[a] ROVGF/*tzv*(+2*df*)[b]	VDE (theoretical)[a] ROVGF/6-311+G(2*df*)[c]
X	6.3–7.2	$5e$	6.65 (0.91)	6.68 (0.91)
		$5a_1$	6.72 (0.91)	6.76 (0.91)
		$4e$	6.83 (0.91)	6.87 (0.91)
		$4a_1$	6.92 (0.91)	6.96 (0.91)
		$1a_2$	6.98 (0.91)	7.00 (0.91)
		$3e$	7.11 (0.92)	7.14 (0.91)
A	7.3–7.9	$2e$	7.50 (0.91)	7.54 (0.91)
		$3a_1$	7.77 (0.91)	7.82 (0.91)

[a]Pole strengths are shown in parentheses.
[b]At the CCSD(T)/*tzv*(+*d*) geometry.
[c]At the CCSD(T)/6-311+G* geometry.

TABLE VIII. Experimental and theoretical vertical detachment energies (VDE) in eV for the $Na_4Cl_5^-$ (C_{4v},$^1A_1$) global minimum structure.

Feature	VDE (expt.)	Molecular orbital	VDE (theoretical)[a]	
			ROVGF/$tzv(+2df)$[b]	ROVGF/6-311+G$(2df)$[c]
X	7.0–7.8	$5e$	7.30 (0.91)	7.28 (0.91)
		$3b_1$	7.32 (0.91)	7.29 (0.91)
		$5a_1$	7.34 (0.91)	7.34 (0.91)
		$4e$	7.40 (0.91)	7.38 (0.91)
		$4a_1$	7.53 (0.91)	7.53 (0.91)
		$1a_2$	7.55 (0.91)	7.57 (0.91)
		$3e$	7.66 (0.91)	7.64 (0.91)
		$1b_2$	7.78 (0.92)	7.76 (0.91)

[a]Pole strengths are shown in parentheses.
[b]At the B3LYP/$tzv(+d)$ geometry.
[c]At the B3LYP/6-311+G* geometry.

ment with the *X* band of the $Na_3Cl_4^-$ PES spectrum [Fig. 1(c)]. Two more detachment channels occur at higher binding energies, which agree with the weaker *A* band in the PES spectrum. The highest occupied molecular orbital (HOMO) of $Na_3Cl_4^-$ is a degenerate orbital ($5e$), which would result in a Jahn-Teller effect upon photodetachment, leading to structural distortions in the ground state of neutral Na_3Cl_4. The broad threshold feature in the PES spectrum of $Na_3Cl_4^-$ is consistent with a structural change between the anion and neutral ground states. The calculated spectral pattern of $Na_4Cl_5^-$ is also very complicated with the eight detachment channels congested within a 0.5 eV energy range (Table VIII). This is in exact agreement with the broadband observed in the PES spectrum [Fig. 1(d)]. The HOMO of $Na_4Cl_5^-$ is also degenerate, similar to that of $Na_3Cl_4^-$, again leading to the relatively broad onset in the PES spectrum due to the Jahn-Teller effect.

Overall, the agreement between the theoretical and experimental VDEs is excellent, confirming unequivocally the identified global minimum structure for the $Na_xCl_{x+1}^-$ clusters.

VIII. CONCLUSIONS

A series of anionic sodium chloride clusters, $Na_xCl_{x+1}^-$ ($x=1-4$), were investigated by *ab initio* genetic algorithm and photoelectron spectroscopy. The global minima found using our GEGA method for heteroatomic systems agree with the previously reported structures obtained by different methods. The finest feature of our algorithm, in contrast to all the methods proposed before, is the *ab initio* quality of the final global minima relative energies and geometries. Experimental photoelectron spectra revealed very high electron binding energies for the anions, which increase from a VDE of 5.6 eV for $NaCl_2^-$ to an extremely high value of 6.9 eV for $Na_4Cl_5^-$. Thus, all these clusters belong to the class of molecules called superhalogens, because their VDEs are substantially higher than the VDEs of the atomic halogen anions. Excellent agreement was obtained between theoretically predicted VDEs for the global mimima and the experimentally observed detachment features, confirming the validity of the global minimum structures identified by the GEGA method. The current work demonstrates the robust applicability of the developed *ab initio* GEGA for relatively simple heteroatomic cluster systems.

ACKNOWLEDGMENTS

The theoretical work done at Utah was supported partially by the donors of The Petroleum Research Fund (ACS-PRF# 38242-AC6), administered by the American Chemical Society and partially by the National Science Foundation (CHE-0404937). The experimental work done at Washington was supported by the National Science Foundation (CHE-0349426) and performed at the W. R. Wiley Environmental Molecular Sciences Laboratory, a national scientific user facility sponsored by DOE's Office of Biological and Environmental Research and located at Pacific Northwest National Laboratory, which is operated for DOE by Battelle.

[1] R. Pflaum, K. Sattler, and E. Recknagel, Chem. Phys. Lett. **138**, 8 (1987).
[2] R. N. Barnett, U. Landman, D. Scharf, and J. Jortner, Acc. Chem. Res. **22**, 350 (1989).
[3] B. I. Dunlap, J. Chem. Phys. **84**, 5611 (1986).
[4] K. K. Sunil and K. D. Jordan, J. Phys. Chem. **91**, 1710 (1987).
[5] E. C. Honea, M. L. Homer, P. Labastie, and R. L. Whetten, Phys. Rev. Lett. **63**, 394 (1989).
[6] C. Ochsenfeld and R. Ahlrichs, J. Chem. Phys. **97**, 3487 (1992).
[7] R. F. W. Bader and J. A. Platts, J. Chem. Phys. **107**, 8545 (1997).
[8] G. L. Gutsev and A. I. Boldyrev, Chem. Phys. Lett. **56**, 277 (1981).
[9] G. L. Gutsev and A. I. Boldyrev, Adv. Chem. Phys. **61**, 169 (1985).
[10] M. K. Scheller and L. S. Cederbaum, J. Phys. B **25**, 2257 (1992).
[11] M. K. Scheller and L. S. Cederbaum, J. Chem. Phys. **99**, 441 (1993).
[12] G. L. Gutsev, R. J. Bartlett, A. I. Boldyrev, and J. Simons, J. Chem. Phys. **107**, 3867 (1997).
[13] H. Hotop and W. C. Lineberger, J. Phys. Chem. Ref. Data **14**, 731 (1985).
[14] X.-B. Wang, C.-F. Ding, L.-S. Wang, A. I. Boldyrev, and J. Simons, J. Chem. Phys. **110**, 4763 (1999).
[15] T. M. Miller and W. C. Lineberger, Int. J. Mass Spectrom. Ion Processes **102**, 239 (1990).
[16] J. E. Campana, T. M. Barlak, R. J. Colton, J. H. DeCorpo, J. R. Wyatt, and B. I. Dunlap, Phys. Rev. Lett. **47**, 1046 (1981).
[17] R. Pfaum, P. Pfau, K. Sattler, and E. Recknagel, Surf. Sci. **156**, 165 (1985).
[18] Y. J. Twu, C. W. S. Conover, Y. A. Yang, and L. A. Bloomfield, Phys. Rev. B **42**, 5306 (1990).
[19] Y. A. Yang, C. W. C. Conover, and L. A. Bloomfield, Chem. Phys. Lett. **158**, 279 (1989).
[20] Y. A. Yang, P. Xia, A. L. Junkin, and L. A. Bloomfield, Phys. Rev. Lett. **66**, 1205 (1991).
[21] P. Xia and L. A. Bloomfield, Phys. Rev. Lett. **72**, 2577 (1994).

[22] N. Yu, P. Xia, L. A. Bloomfield, and M. Fowler, J. Chem. Phys. **102**, 4965 (1995).
[23] D. J. Fatemi, F. K. Fatemi, and L. A. Bloomfield, Phys. Rev. B **55**, 10094 (1997).
[24] P. Dugourd, R. R. Hudgings, and M. F. Jarrold, Chem. Phys. Lett. **267**, 186 (1997).
[25] J. P. K. Doye and D. J. Wales, Phys. Rev. B **59**, 2292 (1999).
[26] N. G. Phillips, C. W. S. Conover, and L. A. Bloomfield, J. Chem. Phys. **94**, 4980 (1991).
[27] A. N. Alexandrova and A. I. Boldyrev (in press).
[28] L. S. Wang, C. F. Ding, X. B. Wang, and S. E. Barlow, Rev. Sci. Instrum. **70**, 1957 (1999).
[29] P. Kebarle and L. Tang, Anal. Chem. **65**, A972 (1993).
[30] S. L. Zhou and M. Hamburger, Rapid Commun. Mass Spectrom. **10**, 797 (1996).
[31] D. R. Zook and A. P. Bruins, Int. J. Mass Spectrom. Ion Processes **162**, 129 (1997).
[32] E. D. Zhang and R. G. Cooks, Int. J. Mass. Spectrom. **195/196**, 667 (2000).
[33] R. G. Parr and W. Yang, *Density-Functional Theory of Atoms and Molecules* (Oxford University Press, Oxford, 1989).
[34] A. D. Becke, J. Chem. Phys. **98**, 5648 (1993).
[35] J. P. Perdew, J. A. Chevary, S. H. Vosko, K. A. Jackson, M. R. Pederson, D. J. Singh, and C. Fiolhais, Phys. Rev. B **46**, 6671 (1992).
[36] A. Schaefer, C. Horn, and R. Ahlrichs, J. Chem. Phys. **97**, 2571 (1992).
[37] A. Schaefer, C. Horn, and R. Ahlrichs, J. Chem. Phys. **100**, 5829 (1994).
[38] J. Cizek, Adv. Chem. Phys. **14**, 35 (1969).
[39] G. D. Purvis III and R. J. Bartlett, J. Chem. Phys. **76**, 1910 (1982).
[40] G. E. Scuseria, C. L. Janssen, and H. F. Schaefer III, J. Chem. Phys. **89**, 7382 (1988).
[41] L. S. Cederbaum, J. Phys. B **8**, 290 (1975).
[42] J. V. Ortiz, J. Chem. Phys. **108**, 1008 (1998).
[43] V. G. Zakrzewski and J. V. Ortiz, Int. J. Quantum Chem. **53**, 583 (1995).
[44] W. von Niessen, J. Shirmer, and L. S. Cederbaum, Comput. Phys. Rep. **1**, 57 (1984).
[45] M. J. Frisch, G. M. Trucks, H. B. Schlegel *et al.*, GAUSSIAN 03, revision A.1, Gaussian, Inc., Pittsburgh, PA, 2003.
[46] M. J. Frisch, G. M. Trucks, H. B. Schlegel *et al.*, GAUSSIAN 98, revision A.7, Gaussian, Inc., Pittsburgh, PA, 1998.
[47] J. H. Holland, *Adaptation in Natural and Artificial Systems* (The University of Michigan Press, Ann Arbor, 1975).
[48] D. E. Goldberg, *Genetic Algorithms in Search, Optimization, and Machine Learning* (Addison-Wesley, Reading, MA, 1989).
[49] L. Davis, *Handbook of Genetic Algorithms* (Van Nostrand Reinhold, New York, 1991).
[50] J. L. Wang, G. H. Wang, and J. J. Zhao, Phys. Rev. B **66**, 035418 (2002).
[51] J. L. Wang, G. H. Wang, and J. J. Zhao, Phys. Rev. A **68**, 013201 (2003).
[52] S. K. Gregurick, M. H. Alexander, and B. Hartke, J. Chem. Phys. **104**, 2684 (1996).
[53] R. P. White, J. A. Niesse, and H. R. Mayne, J. Chem. Phys. **108**, 2208 (1998).
[54] L. M. Marim, M. R. Lemes, and A. Dal Pino, Jr., Phys. Rev. A **67**, 033203 (2003).
[55] K. M. Ho, A. A. Shvartsburg, B. Pan, Z. Y. Lu, C. Z. Wang, J. G. Wacker, J. L. Fye, and M. F. Jarrold, Nature (London) **392**, 582 (1998).
[56] W. Cai, H. Jiang, and X. Shao, J. Chem. Inf. Comput. Sci. **42**, 1099 (2002).
[57] D. P. Stucke, and V. H. Crespi, Nano Lett. **3**, 1183 (2003).
[58] R. L. Haupt and S. E. Haupt, *Practical Genetic Algorithms* (Wiley-Interscience, New York, 1998).
[59] D. M. Deaven and K. M. Ho, Phys. Rev. Lett. **75**, 288 (1995).
[60] Y. Zairi, Phys. Rev. E **51**, R2769 (1995).
[61] J. R. Morris, D. M. Deaven, and K. M. Ho, Phys. Rev. B **53**, R1740 (1996).
[62] A. Tomasulo and M. V. Ramakrishna, J. Chem. Phys. **105**, 10449 (1996).
[63] J. A. Niesse and H. R. Mayne, J. Chem. Phys. **105**, 4700 (1996).
[64] G. M. Wang, E. Blaisten-Barojas, and A. E. Roitberg, J. Chem. Phys. **115**, 3640 (2001).
[65] M. Iwamatsu, J. Chem. Phys. **112**, 10976 (2000).
[66] S. Yoo and X. C. Zeng, J. Chem. Phys. **119**, 1442 (2003).
[67] F. F. Guimaraes, J. C. Belchior, R. L. Johnston, and C. Roberts, J. Chem. Phys. **116**, 8327 (2002).
[68] L. Hui, F. Pederiva, G. H. Wang, and B. L. Wang, J. Chem. Phys. **119**, 9771 (2003).
[69] S. K. Lai, P. J. Hsu, K. L. Wu, W. K. Liu, and M. Iwamatsu, J. Chem. Phys. **117**, 10715 (2002).
[70] V. E. Bazterra, M. B. Ferraro, and J. C. Facelli, J. Chem. Phys. **116**, 5984 (2002).
[71] P. Bobadovaa-Parvanova, K. A. Jackson, S. Srinivas, M. Horoi, C. Kohler, and G. Seifert, J. Chem. Phys. **116**, 3576 (2002).
[72] S. Darby, T. V. Mortimer-Jones, R. L. Johnston, and C. Roberts, J. Chem. Phys. **116**, 1536 (2002).
[73] J. M. Hammersley and D. C. Handscomb, *Monte Carlo Methods* (Methuen, London, 1965), Chap. 9.
[74] H. Kabrede and R. Hentschke, J. Phys. Chem. B **107**, 3914 (2002).
[75] H. Kabrede and R. Hentschke, J. Phys. Chem. B **106**, 10089 (2002).
[76] M. Saunders, J. Comput. Chem. **25**, 621 (2004).
[77] A. I. Boldyrev (unpublished).
[78] K. A. Peterson and J. Koput (unpublished).
[79] I. Anusiewicz and P. Skurski, Chem. Phys. Lett. **358**, 426 (2002).
[80] I. Anusiewicz, M. Sobczyk, I. Dabkowska, and P. Skurski, Chem. Phys. **171**, 291 (2003).
[81] M. Sobczyk, A. Sawicka, and P. Skurski, Eur. J. Inorg. Chem. 3790 (2003).